Korean J. Chem. Eng., 33(2), 473-480 (2016)
DOI: 10.1007/s11814-015-0138-3

pISSN: 0256-1115
eISSN: 1975-7220

High temperature water gas shift reaction over Fe-Cr-Cu nanocatalyst fabricated by a novel method

Seyed Mahdi Latifi† and Alireza Salehirad

Institute of Chemical Technologies, Iranian Research Organization for Science and Technology (IROST), Tehran, Iran
(*Received 6 January 2015 • accepted 29 June 2015*)

Abstract−Fe-Cr-Cu nanocatalyst was synthesized through an inorganic-precursor thermolysis approach and exploited for high temperature water gas shift reaction. The results demonstrated that the method used for the nanocatalyst fabrication led to smaller crystallite size (32.9 nm) and higher BET surface area (127.3 m^2/g) compared to those of a reference sample (65.5 nm, 78.6 m^2/g) prepared by co-precipitation conventional method. Furthermore, the obtained data for catalytic activity showed that the catalyst prepared via inorganic precursor has better activity than the reference sample in all studied temperatures (350-500 °C) and also exhibited higher catalytic activity than a commercial Fe-Cr-Cu catalyst in higher temperatures (more than 450 °C).

Keywords: Water Gas Shift Reaction, Nanocatalyst, Inorganic Precursor, Synthesis, Catalytic Activity

INTRODUCTION

The water gas shift (WGS) reaction is one of the most attractive heterogeneous reactions [1-4] due to applications in ammonia synthesis, adjusting the CO/H_2 ratio in the methanol production and the Fischer-Tropsch synthesis and recently, fuel cell technology. This exothermic reaction is kinetically limited at low temperatures and thermodynamically limited at high temperatures; therefore, it is typically performed in two steps: one at high temperatures (HTS, 300-500 °C), using Fe-Cr-based catalysts [5,6], and the second at low temperatures (LTS, 200-250 °C), using Cu-Zn-based catalysts [7,8].

Magnetite (Fe_3O_4) has been identified as an active component in the HTS conventional catalysts, but during the reaction its activity reduces rapidly owing to the sintering [9]. Therefore, chromium oxide (Cr_2O_3), as a textural promoter, is usually added to the commercial catalysts to increase their stability [10,11]. The commercial HTS catalyst is composed of a small amount of copper to promote its activity and selectivity at lower temperatures [12-16]. The promotional effect of copper is significantly related to the catalyst fabrication approach [17].

The fabrication route can play a key role in the physicochemical properties, and thus the catalytic performance of the WGS catalysts [17]. A few synthetic routes, including co-precipitation (using sodium hydroxide or ammonia as precipitant) [18,19], oxidation-precipitation [16,20], and pyrolysis [21], have been reported to fabricate Fe-Cr-Cu catalysts.

In our previous work [22] high temperature shift Fe-Cr nanocatalyst was prepared via $[Fe(H_2O)_6][Cr(C_2O_4)_3]$, and its catalytic activity was compared with that of an Fe-Cr-Cu commercial catalyst. The results revealed that the CO conversion for the prepared Fe-Cr catalyst reached that of the commercial one only in a narrow range of temperatures (around 500 °C). In this work, to improve the catalytic performance of the HTS nanocatalyst prepared through new facile technique [22], the precursor was modified to $[Fe(H_2O)_6][Cr(C_2O_4)_3]*4H_2O$-nanoCuO. Then, the physicochemical properties and catalytic performance of the nanocatalyst obtained from the thermolysis of the modified precursor were compared to those of a reference sample fabricated from conventional co-precipitation method. In addition to the reference sample, a commercial Fe-Cr-Cu catalyst was also used for more comprehensive comparison of catalytic activities.

MATERIALS AND METHODS

1. Materials

Consumed chemical materials such as $Fe(NO_3)_3*9H_2O$, $Cr(NO_3)_3*9H_2O$ and $Cu(NO_3)_2*3H_2O$ were provided from commercial sources and used without further purification.

2. Precursor Preparation

For $[Fe(H_2O)_6][Cr(C_2O_4)_3]*4H_2O$-nanoCuO precursor fabrication, first, copper oxide nanoparticles and $[Fe(H_2O)_6][Cr(C_2O_4)_3]*4H_2O$ complex were synthesized, and then precursor was obtained via their interaction.

2-1. Synthesis of Copper Oxide Nanoparticles

A 0.5 M sodium hydroxide aqueous solution was added dropwise to a 0.1 M aqueous solution of $Cu(NO_3)_2*3H_2O$ (containing 0.484 g copper nitrate in 20 ml water) until pH 12 was reached. Resulting precipitate was aged for 3 h and then filtered, washed with deionized water, dried and finally calcined at 400 °C for 3 h.

2-2. Synthesis of $[Fe(H_2O)_6][Cr(C_2O_4)_3]*4H_2O$

$[Fe(H_2O)_6][Cr(C_2O_4)_3]*4H_2O$ ion-pair complex was synthesized by reaction of $[Cr(C_2O_4)_3]*3H_2O$ and $Fe(NO_3)_3*9H_2O$ aqueous solutions similarly to the procedure described elsewhere [22].

2-3. Fabrication of $[Fe(H_2O)_6][Cr(C_2O_4)_3]\cdot4H_2O$-nanoCuO Precursor

$[Fe(H_2O)_6][Cr(C_2O_4)_3]*4H_2O$-nanoCuO precursor was fabri-

†To whom correspondence should be addressed.
E-mail: latifi@irost.ir, sm.latifi@yahoo.com

cated by a liquid-phase method and the detailed procedure is as follows: the synthesized copper oxide nanoparticles (0.01 g, 0.125 mmol) were added to an aqueous solution of $[Fe(H_2O)_6][Cr(C_2O_4)_3]*4H_2O$ complex (2.5 g, 4.5 mmol) and the obtained mixture was stirred at 50 °C until dry.

3. Catalyst Fabrication

Fe-Cr-Cu catalysts were fabricated through inorganic precursor approach and co-precipitation method (as a reference). The fabricated catalysts were with molar ratios Fe : Cr 1 : 1 and Fe : Cu 5 : 1.

3-1. Fabrication of Fe-Cr-Cu Nanocatalyst

The Fe-Cr-Cu nanocatalyst was obtained from calcination of the $[Fe(H_2O)_6][Cr(C_2O_4)_3]*4H_2O$-nanoCuO precursor in air using a heating rate of 10 °C/min up to 500 °C and then maintaining at this temperature for 4 h.

3-2. Fabrication of Reference Catalyst

For fabrication of reference catalyst via co-precipitation technique, first, $Fe(NO_3)_3*9H_2O$ (1.33 g, 3.3 mmol), $Cr(NO_3)_3*9H_2O$ (1.32 g, 3.3 mmol) and $Cu(NO_3)_2*3H_2O$ (0.096 g, 0.4 mmol) were dissolved in distilled water to form a mixture of aqueous solutions. Next, an ammonia solution was slowly added to the mixture to adjust pH around 8, which resulted in the precipitation of the hydroxide salts. The obtained precipitate was aged for 6 h under continuous stirring and then filtered and washed several times with deionized water. Finally, the product was dried at 110 °C for 24 h and calcined at 500 °C for 4 h.

4. Sample Characterization

Elemental analysis was determined by a Perkin-Elmer 2400 CHNS/O elemental analyzer. Conductivity reading was obtained by using a Ciba Corning model check-mate 90 conductivity meter. Infrared spectra (4,000-400 cm^{-1}) were measured on an FT-IR PHILIPS, PU9624 spectrophotometer with KBr pellets. Electronic spectra were obtained on a Perkin-Elmer, Lambda 25 spectrophotometer. The metal content of the precursor was measured by atomic absorption spectroscopy using a Varian AA50 equipment. XRD patterns were performed on a Inel-3000 diffractometer using Cu Kα (λ=1.5418 Å) as incident radiation. The BET surface areas and pore volumes of samples were measured with a BELSORB mini model apparatus. Scanning electron microscopy (SEM) of the samples was investigated using the Zeiss Sigma VP SEM equipped with Oxford EDX/WDX detectors.

5. Catalytic Activity Measurements

A stainless steel tube reactor with an inner diameter of 2 mm, equipped with a coiled-around electrical heater and a temperature control system, was used to measure the activity of the studied catalysts (Fig. 1). The reactions were conducted by using 0.8 g (mesh 25-35) catalyst sample, and the influent gas (CO and N_2) flow rates were measured by means of mass flow controllers (7star, Model D07-11c). Precise control of de-ionized water flow rate was achieved via a dosing pump (Milton Roy, Model CEP133-392S3), and the water stream after passing through a vaporizer (400 K) entered the reactor. To homogenize the gas mixture, the inlet portion of the reactor was packed with quartz granules. The reaction product stream after passing through a condenser, was sent to an on-line gas chromatograph (GC) (molecular sieve 5A 80/100) to analyze the CO content. Before reaction, catalyst samples were reduced at 350 °C for 3 h using a H_2/N_2 mixture (50% vol. H_2).

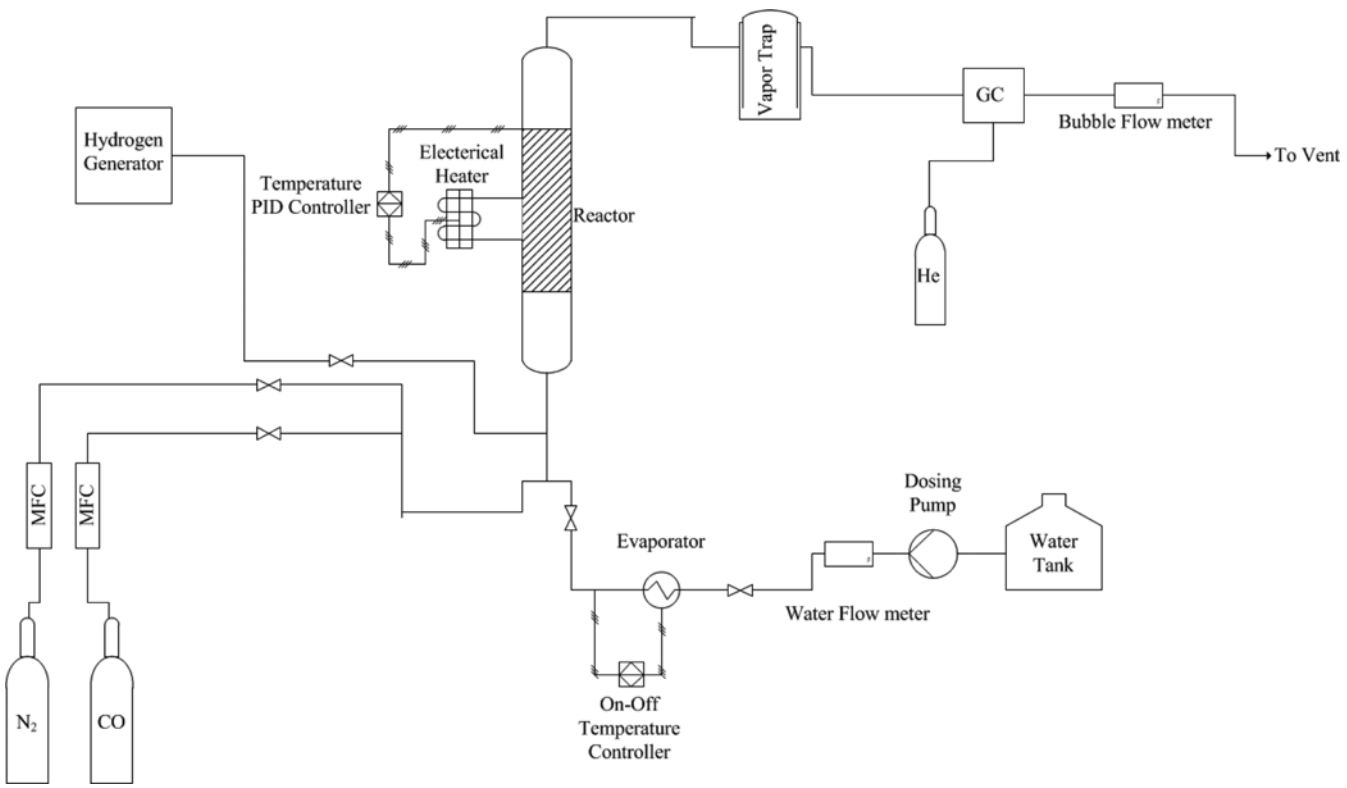

Fig. 1. Experimental setup for catalytic activity measurement.

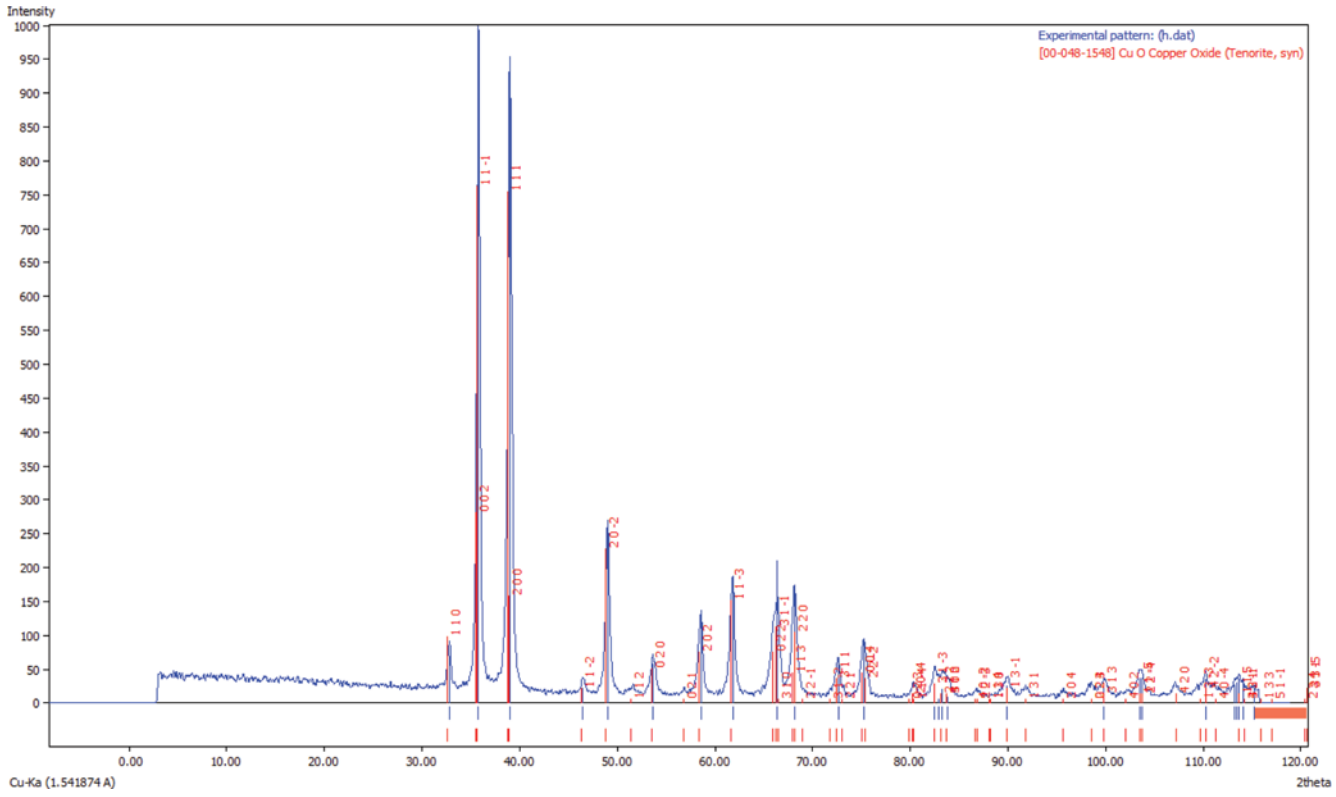

Fig. 2. XRD patterns of CuO nanoparticles.

RESULTS AND DISCUSSION

1. Sample Characterization

The $[Fe(H_2O)_6][Cr(C_2O_4)_3]$*$4H_2O$-nanoCuO precursor is composed of about 88 wt% $[Fe(H_2O)_6][Cr(C_2O_4)_3]$*$4H_2O$ ion-pair complex (containing $[Fe(H_2O)_6]^{3+}$ cationic part and $[Cr(C_2O_4)_3]^{3-}$ anionic part) and 12 wt% CuO nanoparticles.

Structural characterizations of $[Fe(H_2O)_6][Cr(C_2O_4)_3]$*$4H_2O$ ion-pair complex corresponded to the results reported in our previous work [22].

The CuO nanoparticles synthesized by precipitation method were characterized by X-ray diffraction (XRD), scanning electron microscopy (SEM) and energy dispersive X-ray (EDX) techniques. In XRD pattern (Fig. 2) all diffraction lines are assigned to copper oxide phase (JCPDS No. 48-1548). The average crystallite size of copper oxide that was calculated from line broadening of reflections using the Scherrer equation is 17.47 nm. SEM image of copper oxide nanoparticles (Fig. 3) displays spherical particles with sizes of 20-50 nm. Energy dispersive X-ray (EDX) analysis (Fig. 4) shows existence of pure CuO with a molar ratio Cu : O 1 : 1, which is in agreement with XRD results.

XRD patterns of the Fe-Cr-Cu nanocatalyst fabricated via inor-

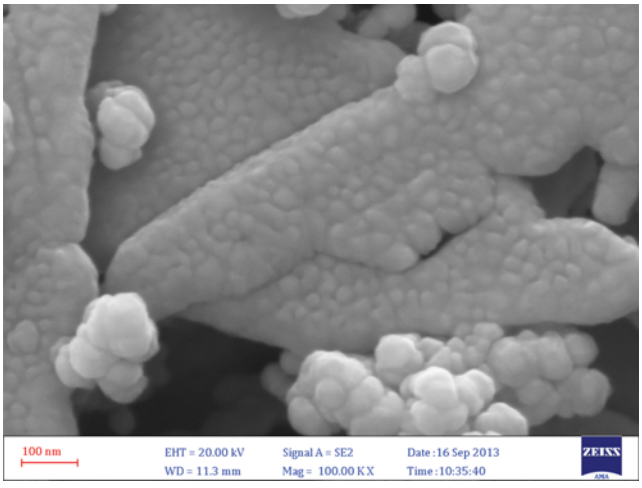

Fig. 3. SEM image for CuO nanoparticles.

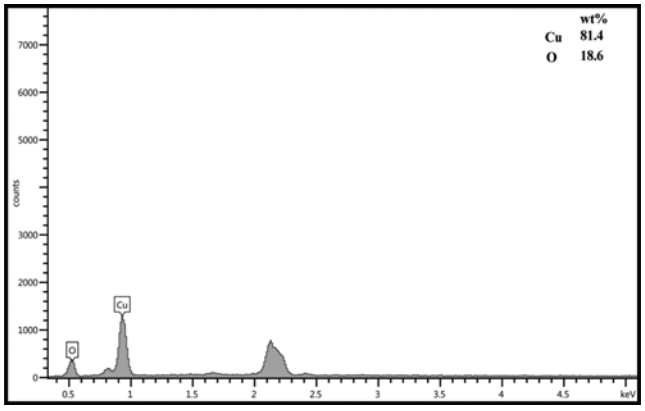

Fig. 4. EDX spectrum of CuO nanoparticles.

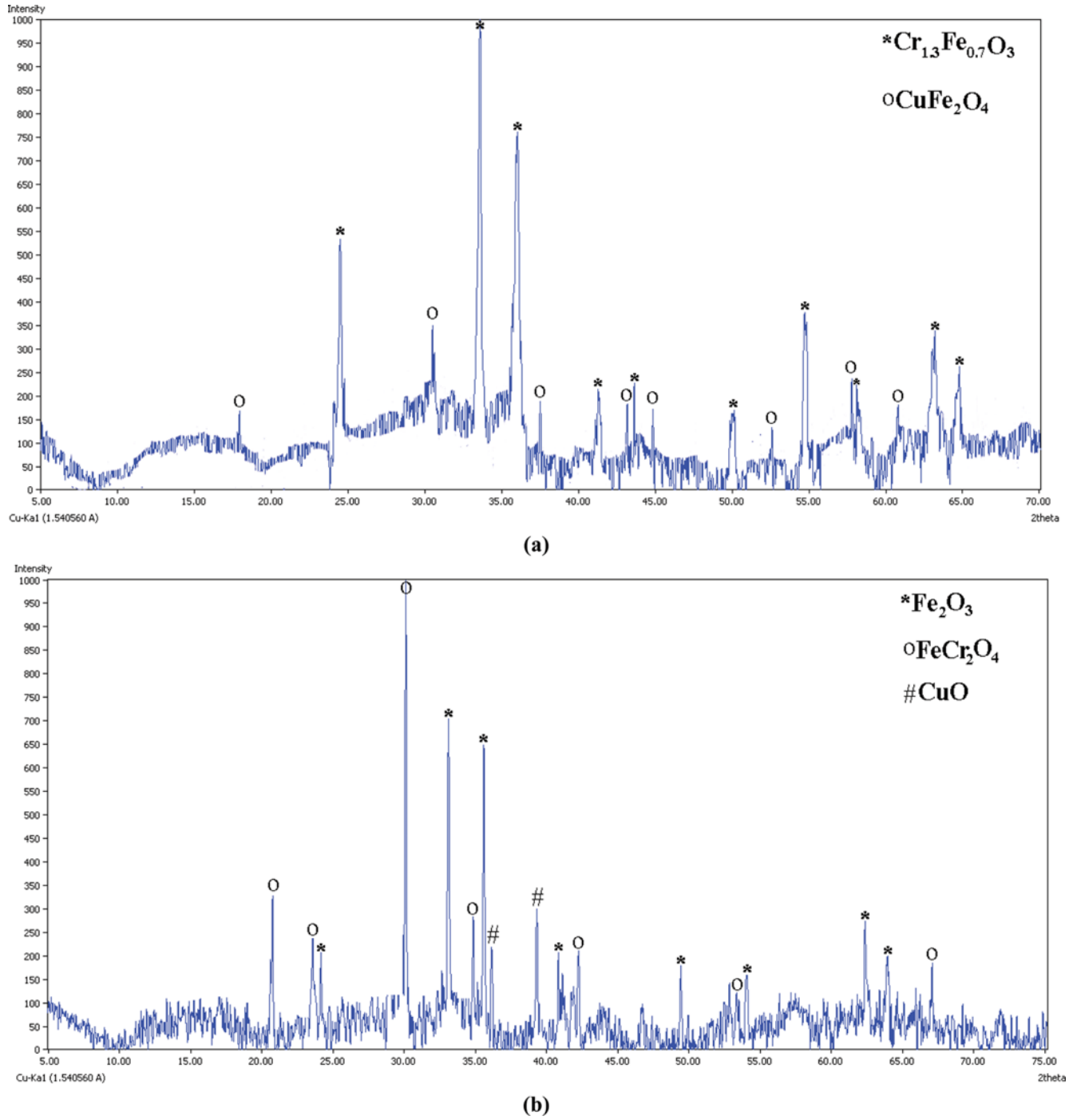

Fig. 5. XRD patterns of Fe-Cr-Cu catalysts (a) fabricated catalyst and (b) reference catalyst.

ganic precursor approach and the reference sample prepared by co-precipitation are displayed in Fig. 5. Reflection lines in the XRD pattern of fabricated nanocatalyst confirm the existence of $Cr_{1.3}Fe_{0.7}O_3$ (JCPDS No. 035-1112) and $CuFe_2O_4$ (JCPDS No. 34-425) phases, indicating that chromium and copper are incorporated into hematite lattice. In addition, the diffraction peaks in the XRD pattern of the reference sample are related to α-Fe_2O_3 (JCPDS No. 033-0664), $FeCr_2O_4$ (JCPDS No. 34-0140) and CuO (JCPDS No. 80-1268) phases. Average crystallite sizes calculated from the XRD peak width at the half height by using the Scherrer equation (Table 1) for the fabricated nanocatalyst and the reference sample were 32.9 and 65.5 nm, respectively, which is in accordance with the SEM results described later.

Fig. 6 shows that the particle sizes for the nanocatalyst and the reference samples are around 30 nm and within the range of 30-100 nm, respectively. Comparing SEM images of the fabricated nanocatalyst and the reference sample revealed that the fabricated nanocatalyst has narrower distribution and smaller particle size, indicating the influence of the fabrication method.

Table 1. Textural properties of the precursor, prepared Fe-Cr-Cu catalyst and reference sample

Sample	BET surface area (m^2/g)	Crystallite size (nm)
$[Fe(H_2O)_6][Cr(C_2O_4)_3]\cdot 4H_2O$-CuO	11.9	
Prepared catalyst	127.3	32.9
Reference catalyst	78.6	65.5

EDX results (Fig. 7) show that the Fe (as active component) composition within the fabricated nanocatalyst is close to the magnitude used during sample synthesis, whereas this is not the case for the reference catalyst.

2. Catalytic Performance

2-1. Residence Time

In continuous catalytic reactions, residence time is usually represented by gas hourly space velocity (GHSV) expressed as

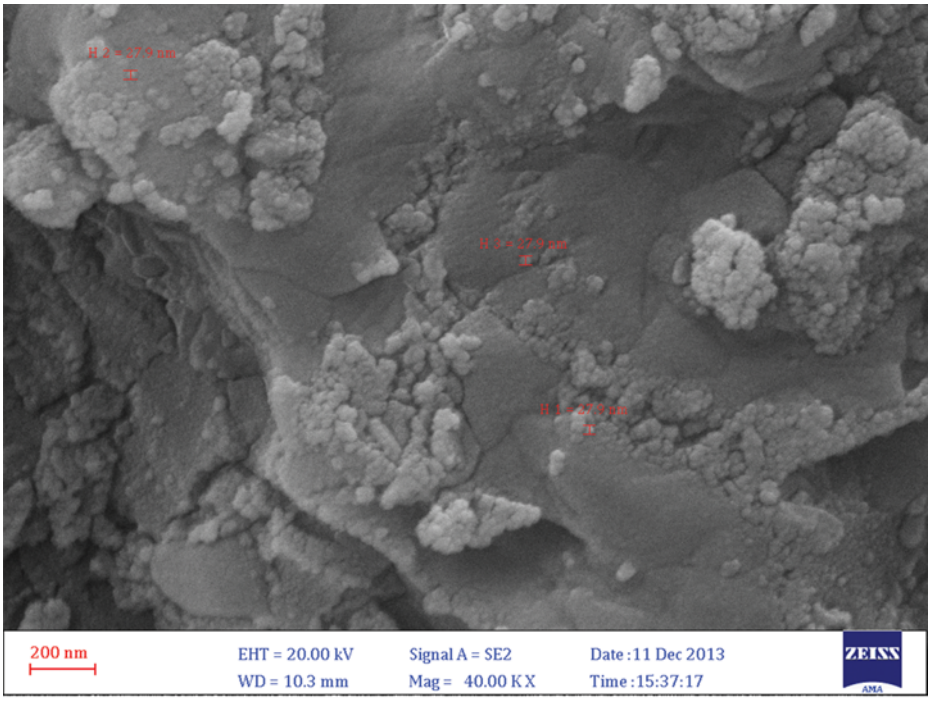

(a)

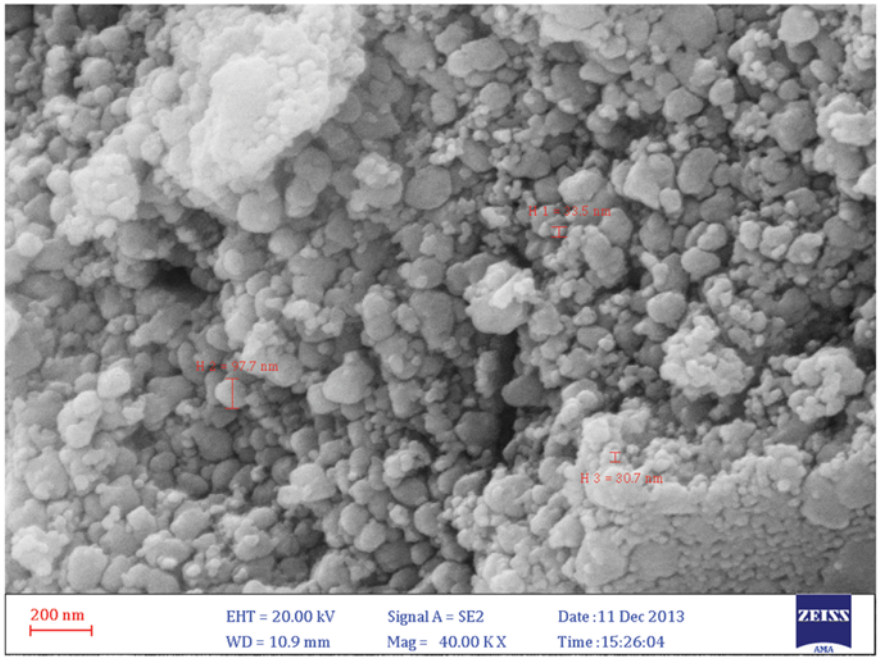

(b)

Fig. 6. SEM images for (a) fabricated catalyst and (b) reference catalyst.

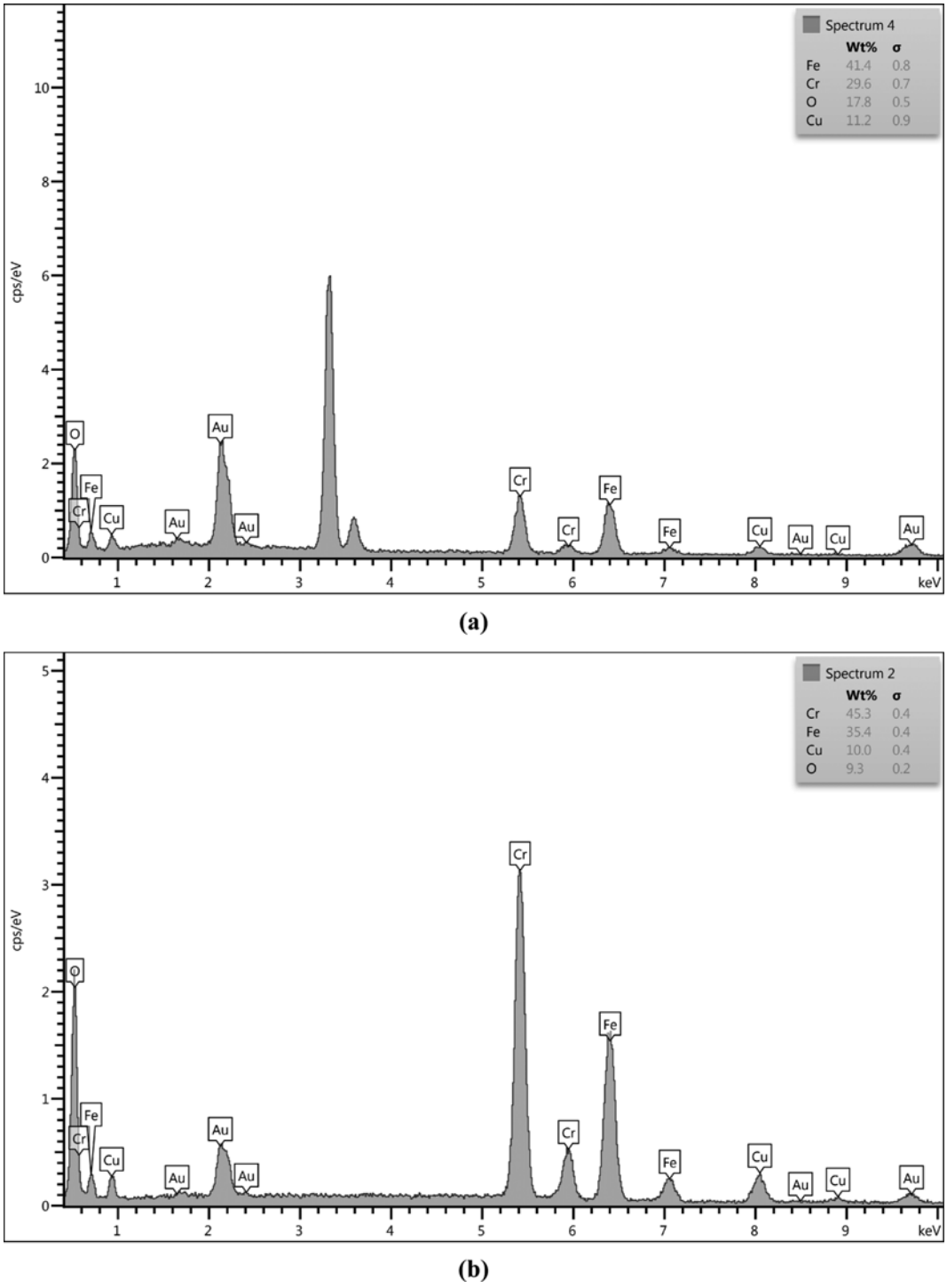

Fig. 7. EDX spectrum of Fe-Cr-Cu catalysts (a) fabricated catalyst (b) reference catalyst.

$$GHSV=(\text{volume flow})/(\text{volume of the catalyst}) \quad (1)$$

In Fig. 8 the CO conversion variation versus the GHSV is shown at 450 °C and the H_2O/CO ratio of 4.8 over the fabricated nano-catalyst. Clearly, in Fig. 8, the CO conversion reduces with increasing GHSV and this decrease is seen to be linear in the results range (36,000 to 134,000 hr^{-1}). The value of 36,000 h^{-1} was adopted for GHSV in the rest of the experiments.

2-2. Effect of Temperature

To compare the catalytic activity of the prepared and the reference catalysts, CO conversion over the catalyst samples was measured at various temperatures at H_2O/CO ratio of 4.8. Also, the activity of the laboratory - fabricated catalysts was compared with that of a commercial Fe-Cr-Cu catalyst along with the Fe-Cr catalyst prepared via an ion-pair complex route [22], and the results are shown in Fig. 9. The catalytic activity of the all catalysts increases

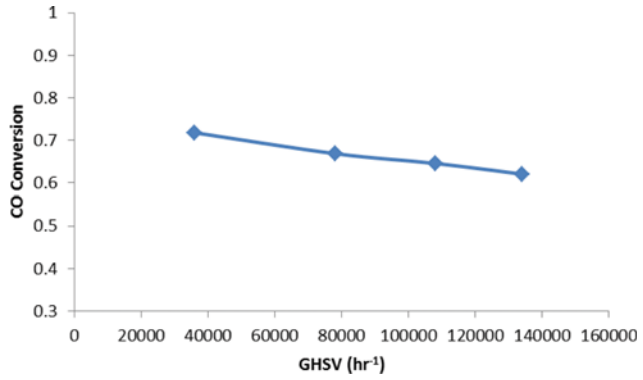

Fig. 8. Effect of GHSV on CO conversion over the fabricated catalyst at 450 °C and H_2O/CO ratio of 4.8.

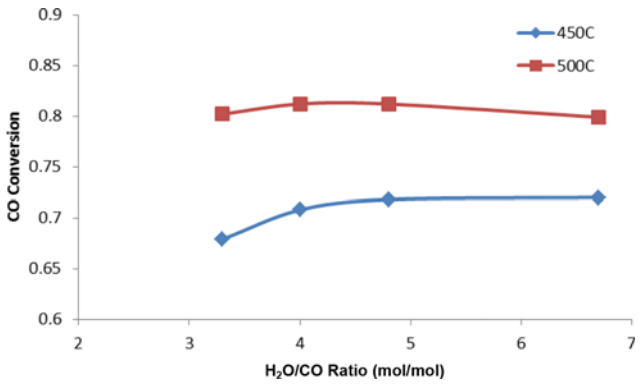

Fig. 10. H_2O/CO ratio influence on the Fe-Cr-Cu nanocatalyst activity in 450 and 500 °C.

with temperature rising, but the extent of these increases differs from one catalyst to another one. The reaction progress over the commercial catalyst experienced a considerable increase from 350 to 400 °C, whereas this breakthrough in CO conversion for the Fe-Cr-Cu nanocatalyst occurred between 400 and 450 °C. This occurrence is observed from 450 to 500 °C for the reference sample, though the catalytic activity of the Fe-Cr nanocatalyst presents almost linear behavior between 400 and 500 °C. From 350 °C to 400 °C the commercial catalyst shows the greatest increase in activity; nevertheless, this catalyst in the temperature range of 400 to 500 °C presents the lowest one. Between 400 to 450 °C, the greatest increase in catalytic activity is for the Fe-Cr-Cu nanocatalyst. In addition, this catalyst displays higher activity than Fe-Cr nanocatalyst and the reference sample in all studied temperatures. Comparison of the results for Fe-Cr and Fe-Cr-Cu nanocatalysts indicates that the modification of the $[Fe(H_2O)_6][Cr(C_2O_4)_3]*4H_2O$ precursor by CuO nanoparticles enhances the catalytic activity of the HTS nanocatalyst in all studied temperatures. Furthermore, in Fig. 9, in a wider range of temperatures, the Fe-Cr-Cu nanocatalyst shows higher catalytic activity than the commercial one, compared to the Fe-Cr sample, as the CO conversion for Fe-Cr-Cu catalyst edges the commercial catalyst in lower temperatures. Also, as observed in Fig. 9, the CO conversion for the Fe-Cr-Cu nanocatalyst is higher than the reference one in all temperatures, which can be attributed to better dispersion of the Fe-Cr-Cu nanocatalyst components, i.e., Fe, Cr and Cu (confirmed by XRD and SEM-EDX results), and having higher BET surface area (due to smaller particle size) compared to the reference sample, indicating the influence of fabrication route.

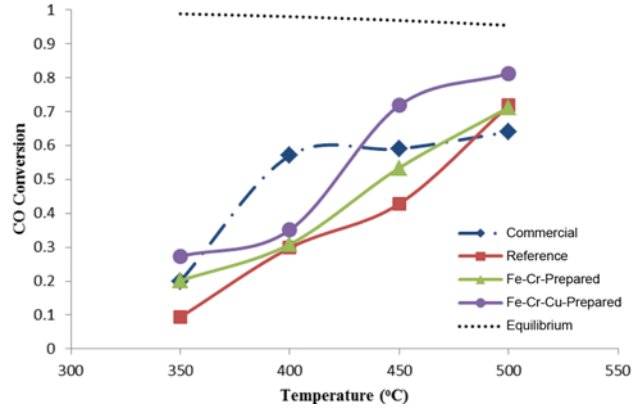

Fig. 9. Temperature effect on the catalyst samples activities.

3. Effect of H_2O/CO Ratio

Fig. 10 demonstrates the effect of H_2O/CO ratio on the Fe-Cr-Cu nanocatalyst activity at 450 and 500 °C.

As depicted in Fig. 10, after a slight increase from the ratio of 3.2 to 4, the CO conversion almost remains constant at 450 °C. Also, variation of H_2O/CO ratio from 3.2 to 6.8 at 500 °C does not have any significant influence on the CO conversion over the Fe-Cr-Cu nanocatalyst.

CONCLUSIONS

The Fe-Cr-Cu nanocatalyst was fabricated via thermolysis of an inorganic-precursor obtained from modification of $[Fe(H_2O)_6][Cr(C_2O_4)_3]*4H_2O$ by adding CuO nanoparticles. Compared with Fe-Cr-Cu prepared from conventional co-precipitation method, this nanocatalyst displays smaller crystallite size and higher BET surface area along with higher catalytic activity for high temperature water gas shift reaction. The CO conversion over the nanocatalyst that resulted from $[Fe(H_2O)_6][Cr(C_2O_4)_3]*4H_2O$-CuO was higher than the Fe-Cr nanocatalyst prepared from $[Fe(H_2O)_6][Cr(C_2O_4)_3]*4H_2O$, suggesting favorable precursor modification. Moreover, the nanocatalyst presents higher catalytic activity than a commercial catalyst in around and more than 450 °C

ACKNOWLEDGEMENT

The authors are thankful to Dr. A. Eliassi and Dr. N. Khandan for their support.

REFERENCES

1. T. Noor, M. V. Gil and D. Chen, *Appl. Catal.*, **B 150-151**, 585 (2014).
2. X. Lin, Y. Zhang, L. Yin, C. Chen, Y. Zhan and D. Li, *Int. J. Hydrogen Energy*, **39**, 6424 (2014).
3. M. K. Gnanamani, G. Jacobs, W. D. Shafer, D. E. Sparks, S. Hopps, G. A. Thomas and B. H. Davis, *Top. Catal.*, **57**, 612 (2014).

4. J. Andersson and J. Lundgren, *Appl. Energy*, **130**, 484 (2014).
5. T. Popa, G. Xu, T. F. Barton and M. D. Argyle, *Appl. Catal. A: Gen.*, **379**, 15 (2010).
6. P. Kappen, J. Grunwaldt, B. S. Hammershoi, L. Troger and B. S. Clausen, *J. Catal.*, **198**, 56 (2001).
7. Z. Bao, W. Ding and Q. Li, *Int. J. Hydrogen Energy*, **37**, 951 (2012).
8. S. Natesakhawat, X. Wang, L. Zhang and U. S. Ozkan, *J. Mol. Catal. A: Chem.*, **260**, 82 (2006).
9. C. Ratnasamy and J. P. Wagnera, *Catal. Rev. Sci. Eng.*, **51**, 325 (2009).
10. F. Meshkani and M. Rezaei, *Korean J. Chem. Eng.*, **32**, 1278 (2015).
11. J. C. Gonzalez, M. G. Gonzalez, M. A. Laborde and N. Moreno, *Appl. Catal.*, **20**, 3 (1986).
12. Y. T. Kim and E. D. Park, *Korean J. Chem. Eng.*, **27**, 1123 (2010).
13. V. Idakiev, A. D. Mihajlova, B. Kunev and A. Andreev, *React. Kinet. Catal. Lett.*, **33**, 119 (1987).
14. C. Rhodes, B. P. Williams, F. King and G. J. Hutchings, *Catal. Commun.*, **3**, 381 (2002).
15. C. Rhodes and G. J. Hutchings, *Phys. Chem. Chem. Phys.*, **5**, 2719 (2003).
16. C. Martos, J. Dufour and A. Ruiz, *Int. J. Hydrogen Energy*, **34**, 4475 (2009).
17. M. Marono, E. Ruiz, J. M. Sanchez, C. Martos, J. Dufour and A. Ruiz, *Int. J. Hydrogen Energy*, **34**, 8921 (2009).
18. G. K. Reddy, K. Gunasekera, P. Boolchand, J. Dong and P. G. Smirniotis, *J. Phys. Chem. C*, **115**, 7586 (2011).
19. F. Meshkani and M. Rezaei, *Chem. Eng. J.*, **260**, 107 (2015).
20. J. Y. Lee, D.-W. Lee, K.-Y. Lee and Y. Wang, *Catal. Today*, **146**, 260 (2009).
21. J. Dufour, C. Martos, A. Ruiz and F. J. Ayuela, *Int. J. Hydrogen Energy*, **18**, 7647 (2013).
22. A. Salehirad, S. M. Latifi and A. Miroliaee, *Mater. Res. Bull.*, **59**, 104 (2014).